



# One-step synthesis of amine-functionalized fluorescent silicon nanoparticles for copper(II) ion detection

Yunqi Wang<sup>1</sup> · Meiling Tian<sup>1</sup> · Wenyue Xie<sup>1</sup> · Chang Ming Li<sup>1</sup> · Yingshuai Liu<sup>1</sup>

Received: 29 March 2019 / Revised: 6 June 2019 / Accepted: 3 July 2019 / Published online: 8 August 2019  
© Springer-Verlag GmbH Germany, part of Springer Nature 2019

## Abstract

Amine-functionalized silicon nanoparticles (A-SiNPs) with intense green fluorescence and photostability are synthesized via a one-step, low-cost hydrothermal method under mild conditions using 3-aminopropyl triethoxysilane (APTES) as a silicon source and L-ascorbic acid (AA) as a reducing reagent. The amine-rich surface not only improves water dispersability and stability of the A-SiNPs but also offers a specific copper(II) ion ( $\text{Cu}^{2+}$ ) coordination capability. The as-prepared A-SiNPs can be directly employed for  $\text{Cu}^{2+}$  detection in “turn-off” mode, resulting from  $\text{Cu}^{2+}$  coordination-induced fluorescence quenching effect. Under optimal conditions,  $\text{Cu}^{2+}$  detection was accomplished with a linear range from 1 to 500  $\mu\text{M}$  and a limit of detection (LOD) at 0.1  $\mu\text{M}$ , which was much lower than the maximum level ( $\sim 20 \mu\text{M}$ ) of  $\text{Cu}^{2+}$  in drinking water permitted by the US Environmental Protection Agency (EPA). In addition, the A-SiNPs were successfully used to detect  $\text{Cu}^{2+}$  in spiked river water, demonstrating its good selectivity and potential application for analysis of surface water samples.

**Keywords** Amine-functionalized silicon nanoparticles ·  $\text{Cu}^{2+}$  detection · Fluorescence quenching effect · Environment monitoring

## Introduction

$\text{Cu}^{2+}$  is a kind of essential trace element, which plays an important role in various biological processes [1, 2].  $\text{Cu}^{2+}$  in water or soil can be directly ingested by human beings or indirectly taken through the food chain. However, over-accumulation of  $\text{Cu}^{2+}$  in human body resulted from high level of  $\text{Cu}^{2+}$  exposure can cause serious physiological damage and various disorders. It has been reported that many neurological diseases such as Alzheimer’s and Wilson’s disease are related to the toxicity of copper.  $\text{Cu}^{2+}$  has been listed as a priority pollutant by the US Environmental Protection Agency (EPA) [3]. Elevated

concentration of  $\text{Cu}^{2+}$  is often found in environment or food due to the wide use of copper in industry, thus resulting in serious and worldwide  $\text{Cu}^{2+}$  pollution [4]. Therefore,  $\text{Cu}^{2+}$  identification and detection is of great importance to monitor and prevent from its pollution.

Currently,  $\text{Cu}^{2+}$  is mainly determined by atomic absorption spectroscopy (AAS), atomic emission spectrometry (AES), and inductively coupled plasma mass spectrometry (ICP-MS) [5–7]. Although these spectral analysis and mass spectrometry analysis offer high sensitivity and good specificity, those techniques require large and expensive instruments and the detection processes are very time-consuming. It is highly desirable for a simple, reliable, and sensitive method for  $\text{Cu}^{2+}$  detection that does not require advanced instruments and experienced professionals. With the explosive development of nanoscience and nanotechnology, more and more nanomaterials have been designed, synthesized, and applied in bio/chemical sensing. ZnS and manganese-doped ZnS quantum dots are utilized as highly selective fluorescent probes for determination of cyanid [8] and sulfur ions [9]. High luminescent carbon dots have been applied as optical probe for  $\text{Cu}^{2+}$  and  $\text{Cr}^{6+}$  detection [10]. In addition, sequential sensing of  $\text{Cu}^{2+}$ , pyrophosphate, and alkaline phosphatase activity was realized with fluorescent upconversion nanoparticle as an optical probe [11].

Silicon nanoparticles (SiNPs), an alternative fluorescent probe, have attracted broad attention in chemical and biological

**Electronic supplementary material** The online version of this article (<https://doi.org/10.1007/s00216-019-02020-9>) contains supplementary material, which is available to authorized users.

✉ Chang Ming Li  
ecmli@swu.edu.cn

✉ Yingshuai Liu  
ysliu@swu.edu.cn

<sup>1</sup> Key laboratory of Luminescent and Real-Time Analytical Chemistry (Southwest University), Ministry of Education, Institute for Clean Energy and Advanced Materials, School of Materials and Energy, Southwest University, No. 2 Tiansheng Road, Beibei, Chongqing 400715, China

research fields owing to its intrinsic advantages, such as low cost, intense fluorescence, low toxicity, good photostability, and water dispersibility [12, 13]. Water-dispersible SiNPs have been prepared via a variety of methods including microwave irradiation, UV irradiation, hydrothermal reaction, and chemical/electrochemical etching treatment [14–16]. Among of them, one-step synthesis of water-dispersible SiNPs under mild condition is the most attractive approach. Heparin sensing and cell imaging have been successfully accomplished using the one-step synthesized amine-functionalized SiNPs (A-SiNP) as an optical probe [17, 18]. Inspired by these works, we synthesized amine-functionalized SiNPs via the one-step green method and directly applied for fluorescent  $\text{Cu}^{2+}$  determination for the first time, eliminating any surface modification with bio-chemical recognition ligands. In this design,  $\text{Cu}^{2+}$  is recognized by the amine group on A-SiNP surface through the specific amine- $\text{Cu}^{2+}$  chelation. A  $\text{Cu}^{2+}$  can coordinate with four amine groups on a same or different A-SiNPs, forming a  $\text{Cu}^{2+}$ -amine complex at a ratio of 1:4 (Fig. 1). The chelation complex formed on A-SiNP surface results in fluorescence quenching by the capture of excited carriers and the interruption of the radiative recombination process [19, 20]. The simple synthesis and surface modification-free merits of the A-SiNPs overcome the challenges faced by the reported nanomaterial-based  $\text{Cu}^{2+}$  sensor.

## Experimental

### Chemicals and reagents

$\text{Cu}(\text{NO}_3)_2 \cdot 3\text{H}_2\text{O}$ ,  $\text{AgNO}_3$ ,  $\text{Ba}(\text{NO}_3)_2$ ,  $\text{Zn}(\text{NO}_3)_2 \cdot 6\text{H}_2\text{O}$ ,  $\text{Mg}(\text{NO}_3)_2 \cdot 6\text{H}_2\text{O}$ ,  $\text{Ca}(\text{NO}_3)_2 \cdot 4\text{H}_2\text{O}$ ,  $\text{Al}(\text{NO}_3)_3 \cdot 9\text{H}_2\text{O}$ ,  $\text{Fe}(\text{NO}_3)_3 \cdot 9\text{H}_2\text{O}$ ,  $\text{MnSO}_4 \cdot 4\text{H}_2\text{O}$ ,  $\text{Co}(\text{NO}_3)_2 \cdot 6\text{H}_2\text{O}$ ,  $\text{Cr}(\text{NO}_3)_3 \cdot 9\text{H}_2\text{O}$ ,  $\text{Hg}$

$(\text{NO}_3)_2 \cdot 2\text{H}_2\text{O}$ ,  $\text{Cd}(\text{NO}_3)_2 \cdot 4\text{H}_2\text{O}$ ,  $\text{NaCl}$ , ascorbic acid (AA), and 3-aminopropyl triethoxysilane (APTES) were purchased from Sigma-Aldrich (Shanghai, China). All of these reagents are of analytical grade and used as received without further purification. Deionized (DI, 18 M $\Omega$ ) water used in all experiments is produced by a water purification system (Q-Grad®1, Millipore).

### Synthesis of A-SiNPs

A-SiNPs were synthesized with a one-step hydrothermal method using APTES as a silicon source and AA as a reducing reagent (Fig. 1) [18]. Specifically, 1.0 mL of APTES was mixed with 4.0 mL DI water under magnetic stirring. 1.25 mL of 0.1 M AA was then injected into the above mixture, following by stirring for 10 min. Finally, the total mixture was incubated under 40 °C for 5 h in a water bath. Continuous magnetic stirring was applied throughout the incubation process. The resultant A-SiNPs were purified through a dialysis procedure to remove the residual APTES and AA, which could affect the follow-up experiments.

### A-SiNP characterization

Excitation and emission spectrum of the prepared A-SiNPs was recorded with a fluorescence spectrometer (Shimadzu, RF-5301PC). Fourier transform infrared (FT-IR) spectra were examined by an FT-IR spectrophotometer (Thermo-Fisher, Nicolet 6700). Ultraviolet-visible (UV-vis) absorption spectra were collected by Shimadzu UV-2550 spectrophotometer. Size and shape of the A-SiNPs were characterized using a transmission electron microscopy (TEM) (JEOL, JEM-2100) with an accelerating voltage of 200 kV. Photostability of the

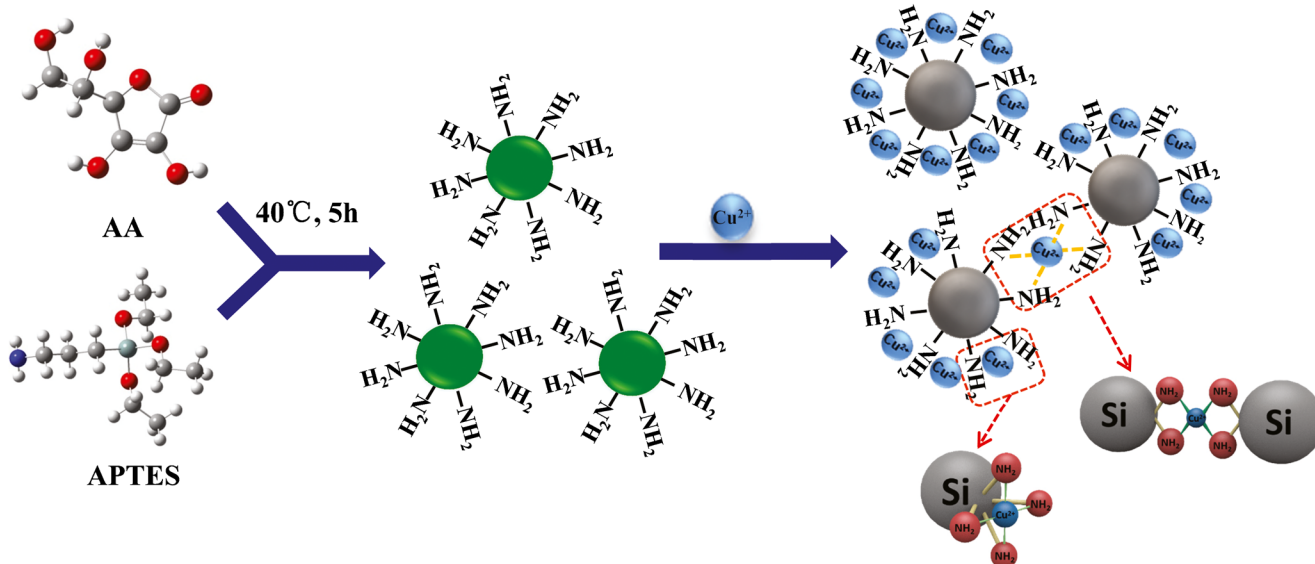


Fig. 1 Schematic illustration of one-step synthesis strategy of A-SiNPs and  $\text{Cu}^{2+}$  detection

prepared A-SiNPs was evaluated under UV irradiation (365 nm). Specifically, 1 mL of the A-SiNP solution in a quartz cuvette was put into a UV analyzer (365 nm, 24W, ZF-20D), where the sample was exposed to UV for 0.5–3 h. The sample was taken out at every half an hour for recording its emission spectrum. A spectrum from the sample without exposure to UV was recorded as a negative control.

### Selectivity of the A-SiNP-based $\text{Cu}^{2+}$ detection under different pH

Selectivity of the A-SiNP-based  $\text{Cu}^{2+}$  detection was first evaluated by testing the signal response to different metal ions including  $\text{Cu}^{2+}$ ,  $\text{Ag}^+$ ,  $\text{Ba}^{2+}$ ,  $\text{Zn}^{2+}$ ,  $\text{Mg}^{2+}$ ,  $\text{Ca}^{2+}$ ,  $\text{Al}^{3+}$ ,  $\text{Fe}^{3+}$ ,  $\text{Mn}^{2+}$ ,  $\text{Co}^{2+}$ ,  $\text{Cr}^{3+}$ ,  $\text{Hg}^{2+}$ , and  $\text{Cd}^{3+}$ . Since  $\text{Hg}^{2+}$  have a significant influence on the experimental results,  $\text{Cl}^-$  with no effect on  $\text{Cu}^{2+}$  detection is introduced to mask its interference. A given amount of A-SiNPs was added into the above metal ion solutions, respectively, resulting in a final concentration at 100  $\mu\text{M}$ . The pH effect on the signal response was also investigated under pH 4.0, 5.0, and 6.0. Under a given pH value, two spectra were recorded from the buffer solutions with and without each testing metal ion, respectively. The signal response is calculated by  $F_0 - F$ , where  $F_0$  is the fluorescence intensity observed from the negative control (without metal ions) and  $F$  is the intensity from the sample with metal ions.

### A-SiNP-based fluorescent detection of $\text{Cu}^{2+}$

A given amount of A-SiNPs was mixed with different levels of  $\text{Cu}^{2+}$ , resulting in final  $\text{Cu}^{2+}$  concentrations at 0.01, 0.05, 0.1, 0.5, 1, 5, 10, 50, 100, and 500  $\mu\text{M}$ . Subsequently, the mixtures were incubated for 30 min at room temperature to allow the coordination between amine at the surface of A-SiNPs and  $\text{Cu}^{2+}$ . The dilution buffer containing same level of A-SiNPs was applied as a negative control. A series of emission spectra were recorded under excitation at 370 nm from the above mixtures. Slit width of 5 nm was chosen for both excitation and emission.

## Results and discussion

### Characterization of the synthesized A-SiNPs

Excitation (a curve) and emission (b curve) spectra of A-SiNPs are shown in Fig. 2a, where a strong excitation peak at 370 nm and a strong PL emission peak at 480 nm are observed, shows that broad absorption in the wavelength region  $< 400$  nm is observed from UV-vis spectrum (Fig. 2a, c curve). The insert is an optical picture of the A-SiNPs under 365 nm UV illumination. The observed blue-green color is in

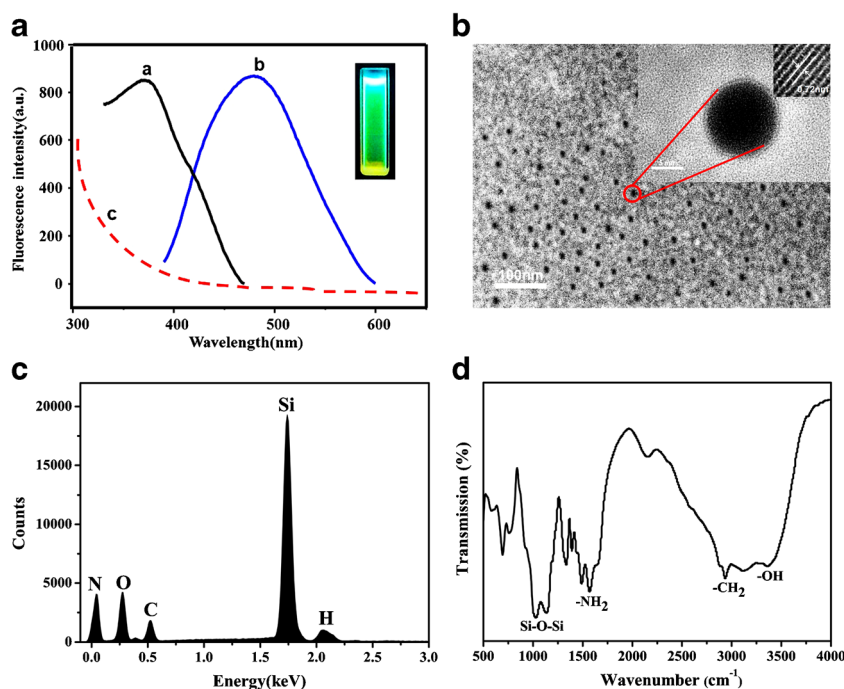
good agreement with the emission spectrum with a peak at around 480 nm. The luminescent properties of the A-SiNPs mainly result from quantum confinement of excitons [21] and defect states [22]. When excited by energy higher than its band gap, electrons are excited from the ground state to the excited state, and photons are generated due to the radiative recombination process. In the A-SiNP nanocrystal, the electron-hole recombination rate increases due to the increased overlap of the electron and hole wave functions confined in the nanodot, while the nonradiative recombination rate is reduced at the same time, thus resulting in enhanced fluorescence emission. In addition, defect states at interface or in the nanocrystal also play a critical role in A-SiNP emission [16]. These defect states mainly come from incomplete hydrolyzation of APTES, the low crystallinity of silicon core, and the doping of impurities.

Size and morphology of the as-prepared A-SiNPs was first characterized by TEM. As shown in Fig. 2b, the synthesized A-SiNPs are monodispersed particles with reasonably uniform size and spherical shape. Based on statistical analysis, average diameter of the A-SiNPs is around 13.7 nm. Elemental analysis of the A-SiNPs was carried out using energy-dispersive X-ray (EDX) spectroscopy. Figure 2c shows that Si, C, N, H, and O elements are observed from the synthesized A-SiNPs. Zeta potential, which is closely related to surface charge of the nanoparticles in a liquid solution, of the prepared SiNPs is measured with Nano-ZS Zetasizer ZEN 3600 (Malvern Instruments Ltd., UK). A positive zeta potential + 15.4 mV is observed from the A-SiNPs, indicating that positive charges present on their surface. It is obviously attributed to the amine groups coming from APTES. An FT-IR spectrum was recorded from the synthesized SiNP to determine functional groups on its surface (Fig. 2d). The broad feature between 3000 and 3500  $\text{cm}^{-1}$  should be assigned to the  $-\text{OH}$  stretching. The bands at 2870 and 2920  $\text{cm}^{-1}$  are attributed to the stretching vibrations of  $\text{CH}_2$ . The sharp absorbance peak at 1000–1200  $\text{cm}^{-1}$  corresponds to the vibrational stretch of  $\text{Si}-\text{O}-\text{Si}$  bonding. The strong bands at 1565 and 1632  $\text{cm}^{-1}$  are assigned to asymmetric and symmetric bending of the primary amine ( $-\text{NH}_2$ ), confirming the presence of amine group on the synthesized A-SiNPs.

### Effect of different parameters on A-SiNP fluorescence

The water-dispersible A-SiNPs were synthesized through a facile one-step hydrothermal method with APTES as a precursor, which was reduced by the reducing agent AA. At a given concentration of APTES and AA, the incubation time plays a very important role in the synthesis. We synthesized six batches of A-SiNPs by varying the incubation time from 0.5 to 5 h. With the prolongation of incubation time, the solution color changes from pink to red to orange as shown in Fig. 3a, while the fluorescence intensity increases gradually

**Fig. 2** **a** Fluorescent excitation/emission spectra (a/b curve) and UV-vis absorption (c curve) of the A-Si NPs. Insert: optical picture of the A-SiNP suspension under 365 nm illumination. **b** TEM image of the A-SiNPs. **c** EDX pattern of the A-SiNPs. **d** FT-IR spectra of the A-SiNPs



and the highest intensity is observed at 5 h. Theoretically, the incubation time is closely related to the reaction efficiency. Under continuous stirring, more and more A-SiNPs are produced in the solution with the prolongation of incubation time, thus resulting in the color become deeper and deeper. In addition, size and shape of the synthesized A-SiNPs become more and more uniform with the increase of reaction time, indicating that crystallization of the A-SiNPs is improved. The time-dependent increase of fluorescence intensity is apparently ascribed to the gradual accumulation and the improved crystallization of A-SiNPs. As shown in Fig. 3b, with the increase of excitation wavelength from 370 to 450 nm, the fluorescence intensity of the A-SiNPs gradually decreases, and at the same time, a red shift of the emission peaks is clearly observed. Based on above results, 370 nm is considered as the optimal excitation [23, 24]. Thus, excitation at 370 nm is chosen in the

following experiments. Photostability of the synthesized A-SiNPs was investigated by UV irradiation for a given time from 0.5 to 3 h. Although the fluorescence intensity decreases gradually with the increase of irradiation time, more than 60% of the original signal intensity still remains after 3 h UV irradiation (Fig. 3c), indicating its reasonably good photostability.

In order to explore the effect of buffer acidity on the A-SiNP emission, diluted hydrochloric acid was applied to adjust pH of the A-SiNP solution. A series of pH values ranging from 2.0 to 10.0 was achieved. Then fluorescence spectra and signal intensities were recorded from the above samples via fluorescence spectrometer and microplate reader. Figure 4a shows that peak values of the emission recorded by the fluorescence spectrometer increase first and then decrease with pH increment from 2.0 to 10.0. The highest signal intensity is observed at pH 6.0. Similar results are achieved by use of

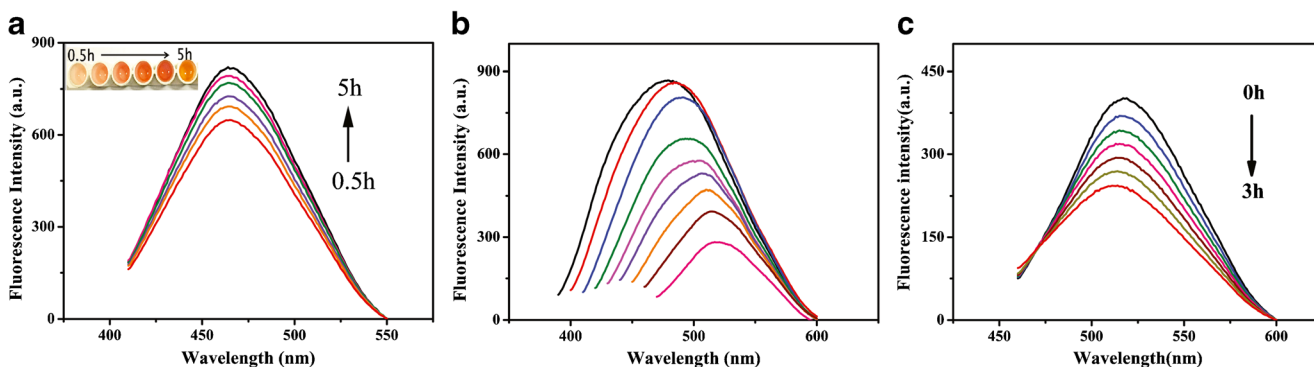


**Fig. 3** **a** Fluorescence spectra recorded from the A-SiNP solutions obtained at 0.5, 1, 2, 3, 4, and 5 h incubation. Insert: optical image of the resulted A-SiNP solution. From left to right, the incubation time is 0.5, 1, 2, 3, 4, and 5 h. **b** Emission spectra of the A-SiNPs observed under

different excitations from 370 to 450 nm with 10 nm step increase. **c** Fluorescence spectra of A-SiNP solution after UV irradiation for 0.5, 1, 1.5, 2, 2.5, and 3 h

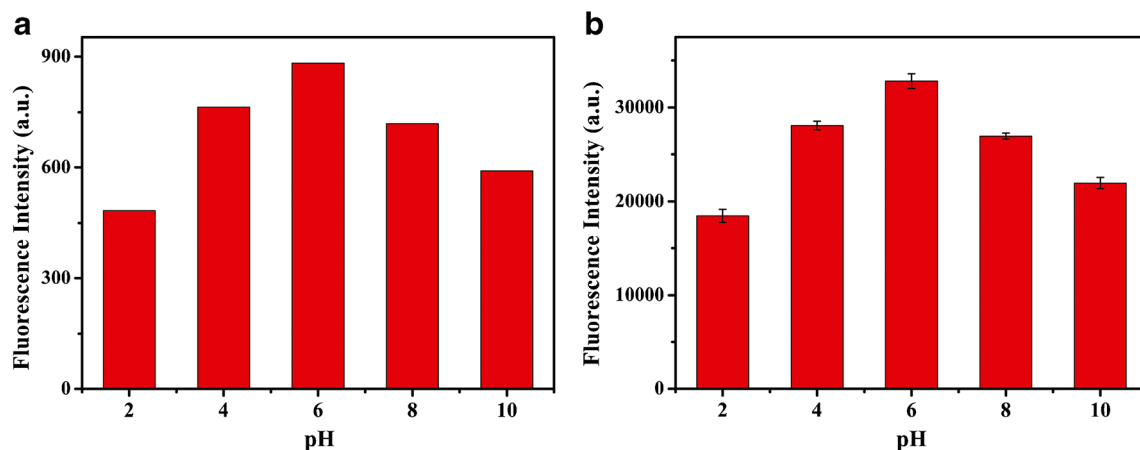


**Fig. 4** pH-dependent fluorescence emission from A-SiNPs. After stirring for 5 h at 40 °C, fluorescence emissions are measured from the obtained samples under pH 2.0, 4.0, 6.0, 8.0, and 10.0. pH-dependent fluorescence

intensity of A-SiNPs excited at 380 nm is recorded by a fluorescence spectrometer (a) with detection range of 0–1000 and by a microplate reader (b) with detection range of 0–55000

microplate reader (Fig. 4b), further confirming the pH effect on A-SiNP fluorescence properties. This phenomenon is probably ascribed to the different protonation ratio of amine group at various pH. The lower solution pH is, the higher level protonation of amine group is resulted, leading to decrease of fluorescence emission. However, the protonation ratio of surface amine group decreases gradually with further increase of solution pH (pH > 6.0). In this case, net surface charge could be reduced due to the low protonation ratio, resulting in possible A-SiNP aggregation and poor fluorescence emission. Therefore, the highest fluorescence emission is observed from A-SiNP solution with a pH 6.0 [25].

### Selectivity of A-SiNP-based Cu<sup>2+</sup> detection

Anti-interference capability is one of the most important performances of chemo/biosensors. In this case, pH not only affects fluorescence emission of the A-SiNPs, as discussed in the “Effect of different parameters on A-SiNP fluorescence” section, but also influences the chelation ability of amine group to metal ions. Amine groups are unable to form complex with Cu<sup>2+</sup> under pH ≤ 3.0 because of the over protonation, while Cu<sup>2+</sup> is unstable in alkaline solutions (pH >

7.0) due to its hydrolysis. As we know,  $K_{sp}[\text{Cu}(\text{OH})_2]$  is  $2 \times 10^{-19}$ , when the pH value is 6.0, the  $Q_C$  value (solubility products) of Cu<sup>2+</sup> at 100 μM is  $1 \times 10^{-20}$ ,  $Q_C < K_{sp}$ . Therefore, the precipitation of Cu<sup>2+</sup> is not possible at concentration of 100 μM under pH 6.0. To explore the best pH value in Cu<sup>2+</sup> detection, interference from various metal ions including Ag<sup>+</sup>, Ba<sup>2+</sup>, Zn<sup>2+</sup>, Mg<sup>2+</sup>, Ca<sup>2+</sup>, Al<sup>3+</sup>, Fe<sup>3+</sup>, Mn<sup>2+</sup>, Co<sup>2+</sup>, Cr<sup>3+</sup>, Hg<sup>2+</sup>, and Cd<sup>3+</sup> was investigated under pH 4.0–6.0. Figure 4 shows that Cu<sup>2+</sup> results in the highest quenching effect of the A-SiNPs over other metal ions under all pH values from 4.0 to 6.0. An obvious response to Hg<sup>2+</sup> is also observed from the sensing platform. In order to inhibit the interference from Hg<sup>2+</sup>, Cl<sup>−</sup> with no effect on Cu<sup>2+</sup> detection was introduced to the sensing system to mask Hg<sup>2+</sup>. As shown in Fig. 5, only a negligible response is observed from Hg<sup>2+</sup> in the group treated with Cl<sup>−</sup> in comparison to the test without Cl<sup>−</sup>. The result indicates that Hg<sup>2+</sup> interference is efficiently masked by the introduction of Cl<sup>−</sup>. Although HgCl<sub>2</sub> is soluble in water, a chelation complex [HgCl<sub>4</sub>]<sup>2−</sup> can be formed in the presence of abundant Cl<sup>−</sup> [26], resulting in significant decrease of free Hg<sup>2+</sup> level in the detection system. Therefore, the Cl<sup>−</sup>-induced masking effect is apparently attributed to the formation of [HgCl<sub>4</sub>]<sup>2−</sup>. The change percentage in the signal

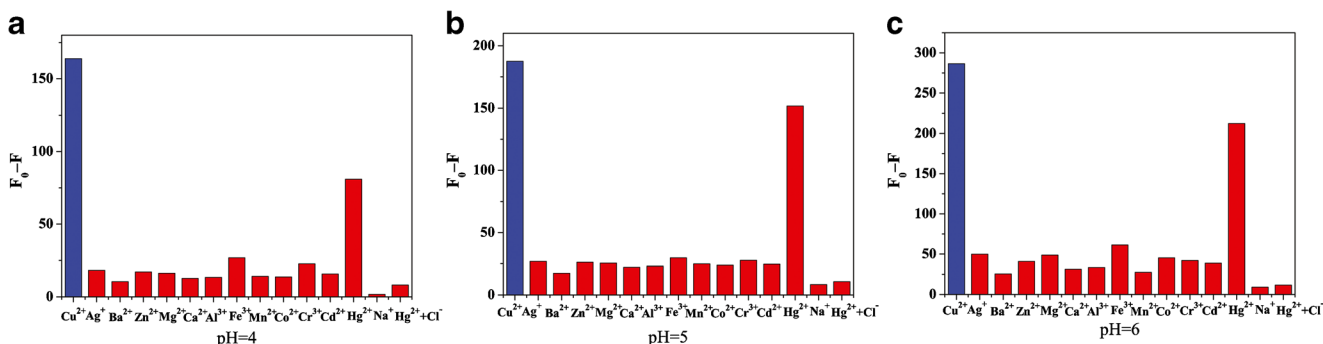


**Fig. 5** Different metal ion-induced quenching effect of A-SiNPs under pH 4.0 (a), 5.0 (b), and 6.0 (c). The concentration of all metal ions is 100 μM

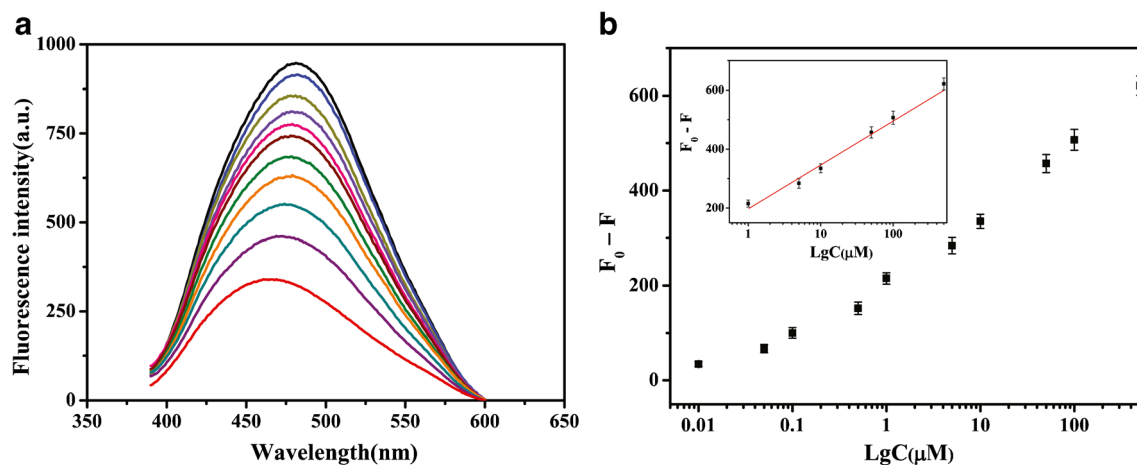


**Fig. 6** **a** Emission spectra of A-SiNPs in presence of  $\text{Cu}^{2+}$  with concentrations at 0.01, 0.05, 0.1, 0.5, 1, 5, 10, 50, 100, and 500  $\mu\text{M}$ . **b** The plot of  $F_0 - F$  at 480 nm against  $\text{Cu}^{2+}$  concentrations at 0.01, 0.05, 0.1, 0.5, 1, 5,

10, 50, 100, and 500  $\mu\text{M}$ . Insert: the plot of  $F_0 - F$  at 480 nm against  $\text{Cu}^{2+}$  concentrations at 1, 5, 10, 50, 100, and 500  $\mu\text{M}$

intensity for these interfering metal ions has been presented in Table S1 in the Electronic Supplementary Material (ESM). Taking into account of pH effect, the lowest interference is observed from the metal ions  $\text{Ag}^+$ ,  $\text{Ba}^{2+}$ ,  $\text{Zn}^{2+}$ ,  $\text{Mg}^{2+}$ ,  $\text{Ca}^{2+}$ ,  $\text{Al}^{3+}$ ,  $\text{Fe}^{3+}$ ,  $\text{Mn}^{2+}$ ,  $\text{Co}^{2+}$ ,  $\text{Cr}^{3+}$ , and  $\text{Cd}^{3+}$  under pH 6.0 (Fig. 5c), which is chosen as an optimal condition in following experiments.

### A-SiNP-based $\text{Cu}^{2+}$ detection in lab buffer

In order to investigate performance of the developed sensing strategy,  $\text{Cu}^{2+}$  with concentrations ranging from 0 to 500  $\mu\text{M}$  is analyzed by use the SiNPs as an optical probe under the optimal condition. As shown in Fig. 6a, fluorescence intensity of the A-SiNPs gradually decreases with the increase of  $\text{Cu}^{2+}$  concentration. The quenching effect is ascribed to the inner filter effect of  $\text{Cu}^{2+}$ -amine complexes formed at the surface of the A-SiNPs which absorbs both excitation at 370 nm and emission light of the A-SiNPs at 480 nm [27]. The quenching effect is described with  $F_0 - F$ , where  $F_0$  is the fluorescence intensity recorded from the control sample and  $F$  is the intensity observed from the testing samples. Figure 6b shows a

dose-dependent curve plotted with  $F_0 - F$  as a function of  $\text{Cu}^{2+}$  concentration in the range from 0.1 to 500  $\mu\text{M}$ .

A very good linear relationship ( $R^2 = 0.998$ ) is achieved in the range from 1 to 500  $\mu\text{M}$  (Fig. 6b, insert). An LOD is determined to be 0.1  $\mu\text{M}$  according to the definition of  $\text{Mb} + 3\text{Sd}$ , where Mb and Sd is the mean signal and standard deviation of the negative control, respectively. The LOD is much lower than the maximum level of  $\text{Cu}^{2+}$  ( $\sim 20$   $\mu\text{M}$ ) in drinking water permitted by US Environmental Protection Agency (EPA). In addition, intra-day and inter-day statistical tests for A-SiNP-based  $\text{Cu}^{2+}$  detection were carried out respectively to evaluate the sensing reliability. The variations for both intra-day and inter-day tests are less than 5% (ESM, Fig. S1), indicating a good reliability of the sensing platform. In terms of dynamic range and LOD, the proposed method shows a better performance in comparison with previously reported works. A detailed comparison is listed in Table 1.

### $\text{Cu}^{2+}$ detection in river water

Applicability of the A-SiNP-based  $\text{Cu}^{2+}$  sensing system for practical application is further validated by accomplishing  $\text{Cu}^{2+}$  detection in surface water collected from the Jialing

**Table 1** A comparison of the sensing performance between the proposed method and reported ones

Detection method	LOD	Dynamic range	pH	Response time	Selectivity	Ref.
Atomic absorption spectroscopy	0.102 $\mu\text{M}$	0.1–20 $\mu\text{M}$	pH = 9	60 min	$\text{Cu}^{2+}$ , $\text{Hg}^{2+}$ , $\text{Fe}^{3+}$	[28]
Atomic emission spectrometry	1 $\mu\text{M}$	1–20 $\mu\text{M}$	pH = 4	15 min	$\text{Cu}^{2+}$ , $\text{Al}^{3+}$ , $\text{Mn}^{2+}$	[29]
Inductively coupled plasma mass spectrometry	0.154 $\mu\text{M}$	0.15–4 $\mu\text{M}$	pH = 6	30 min	$\text{Cu}^{2+}$ , $\text{Pb}^{2+}$ , $\text{Th}^{3+}$	[30]
CdSe/ZnS quantum dots	1.1 $\mu\text{M}$	1–40 $\mu\text{M}$	pH = 5.5	10 min	$\text{Cu}^{2+}$ , $\text{Hg}^{2+}$	[31]
Cyclam-functionalized carbon nanoparticles	0.1 $\mu\text{M}$	0.1–4 $\mu\text{M}$	pH = 7.4	5 min	$\text{Cu}^{2+}$ , $\text{S}^{2-}$	[32]
ZnO nanoparticles	15.7 $\mu\text{M}$	10–1000 $\mu\text{M}$	pH = 9.2	30 min	$\text{Cu}^{2+}$ , $\text{Hg}^{2+}$	[33]
A-SiNP-based detection	0.1 $\mu\text{M}$	0.1–500 $\mu\text{M}$	pH = 6	30 min	$\text{Cu}^{2+}$ , $\text{Hg}^{2+}$	This work

**Table 2** Cu<sup>2+</sup> detection in spiked river water by the proposed method and ICP-MS

	Added	Found by proposed method	Found by ICP-MS	Recovery	RSD ( <i>n</i> = 3)
S1	0	147.41 nM	147 nM	100.21%	0.53%
S2	50 μM	50.94 μM	50.26 μM	101.35%	1.47%
S3	200 μM	203.21 μM	204.42 μM	99.42%	1.68%

River (Chongqing, China). The standard addition method is applied in this experiment. To avoid the interference from particulate matters or impurities, the river water is first filtered through a 0.22-μM membrane and then centrifuged for 20 min at 13000 rpm. The effect of filtration and centrifugation on the final results was evaluated by detection of Cu<sup>2+</sup> in treated and non-treated river water. Negligible effect was observed from the treatment (ESM, Fig. S2). Three samples including river water (S1), river water + 50 μM Cu<sup>2+</sup> (S2), and river water + 200 μM Cu<sup>2+</sup> (S3) were then measured by the proposed method and the well-known ICP-MS. Experimental results are presented in Table 2. Recoveries of 99.42–101.35% and RSD of 0.53–1.68% are achieved from these measurements (Table 2), demonstrating that the proposed method is applicable for Cu<sup>2+</sup> detection in real water samples.

## Conclusions

In conclusion, a sensitive and selective determination of Cu<sup>2+</sup> is accomplished based on fluorescent A-SiNPs, which are synthesized by a green, low-cost, and one-pot method under mild condition. The A-SiNPs demonstrate good water dispersibility, intense fluorescence, and high photostability. Cu<sup>2+</sup>-induced selective quenching phenomenon is observed due to the filter effect from Cu<sup>2+</sup>-amine complexes formed at the surface of A-SiNPs, providing a new and reliable optical probe for fluorimetric Cu<sup>2+</sup> sensing in aqueous media. Under optimal condition, a dynamic range from 1 to 500 μM and an LOD at 0.1 μM is determined, respectively. Furthermore, a real water sample from the Jialing River is successfully analyzed using the developed fluorescent A-SiNP probe, demonstrating its great potential for practical applications.

**Funding** This work is financially supported by the National Natural Science Foundation of China (Grant 21475106), the Fundamental Research Funds for the Central Universities (Grant XDJK2016A010, XDJK2018B004), Chongqing Key Laboratory for Advanced Materials and Technologies of Clean Energies (Grant cstc2011pt), and Chongqing Engineering Research Center for Micro-Nano Biomedical Materials and Devices, Southwest University, China.

## Compliance with ethical standards

**Conflict of interest** The authors declare that they have no conflict of interest.

## References

- Montalti M, Prodi L, Rampazzo E, et al. Dye-doped silica nanoparticles as luminescent organized systems for nanomedicine. *Chem Soc Rev*. 2014;43(12):4243–68.
- Chevigny C, Dalmas F, Cola ED, et al. Polymer-grafted-silicon nanoparticles nanocomposites: dispersion, grafted chain conformation, and rheological behavior. *Macromolecules*. 2017;44(1):122–33.
- Peng J, Liu G, Yuan D, et al. A flow-batch manipulated AgNPs based SPR sensor for colorimetric detection of copper ions (Cu<sup>2+</sup>) in water samples. *Talanta*. 2017;167:310–6.
- Plano LMD, Scibilia S, Rizzo MG, et al. Direct conjugation of silicon nanoparticles with M13pVIII-engineered proteins to bacteria identification. *Appl Phys A*. 2018;124(11):787.
- Almeida JS, Souza OCCO, Teixeira LSG. Determination of Pb, Cu and Fe in ethanol fuel samples by high-resolution continuum source electrothermal atomic absorption spectrometry by exploring a combination of sequential and simultaneous strategies. *Microchim Acta*. 2017;137:22–6.
- Yu J, Yang S, Lu Q, et al. Evaluation of liquid cathode glow discharge-atomic emission spectrometry for determination of copper and lead in ores samples. *Talanta*. 2017;164:216.
- Hachmöller O, Aichler M, Schwamborn K, et al. Investigating the influence of standard staining procedures on the copper distribution and concentration in Wilson's disease liver samples by laser ablation-inductively coupled plasma-mass spectrometry. *J Trace Elem Med Biol*. 2017;44:71–5.
- Shamsipur M, Rajabi HR. Pure zinc sulfide quantum dot as highly selective luminescent probe for determination of hazardous cyanide ion. *Mater Sci Eng C*. 2014;36(1):139–45.
- Rajabi HR, Shamsipur M, Khosravi AA, et al. Selective spectrofluorimetric determination of sulfide ion using manganese doped ZnS quantum dots as luminescent probe. *Spectrochim Acta A*. 2013;107:256–62.
- Liu Y, Zhao Y, Zhang Y. One-step green synthesized fluorescent carbon nanodots from bamboo leaves for copper (II) ion detection. *Sensors Actuators B Chem*. 2014;196(2):647–52.
- Qiu HJ, Guan Y, Luo P, et al. Recent advance in fabricating monolithic 3D porous graphene and their applications in biosensing and biofuel cells. *Biosens Bioelectron*. 2017;89:85–95.
- De CLT, Domínguezberrocal L, Murguía JR, et al. ε-Polylysine-capped mesoporous silica nanoparticles as carrier of the C9h peptide to induce apoptosis in cancer cells. *Chem Eur J*. 2018;24(8):1890.
- Colino C, Millán C, Lanao J. Nanoparticles for signaling in biodiagnosis and treatment of infectious diseases. *Int J Mol Sci*. 2018;19(6):1627.
- Natarajan R, Bridgland L, Sirikulkajorn A, et al. Tunable porous organic crystals: structural scope and adsorption properties of nanoporous steroidal ureas. *J Am Chem Soc*. 2013;135(45):16912–25.
- Zhong Y, Sun X, Wang S, et al. Facile, large-quantity synthesis of stable, tunable-color silicon nanoparticles and their application for long-term cellular imaging. *ACS Nano*. 2015;9(6):5958–67.

16. Liang C, Lin C, Cheng T, et al. Nanoimprinting: nanoimprinting of flexible polycarbonate sheets with a flexible polymer mold and application to superhydrophobic surfaces. *Adv Mater Interfaces*. 2015;2(7).
17. Gong WL, Wang B, Aldred MP, et al. Tetraphenylethene-decorated carbazoles: synthesis, aggregation-induced emission, photo-oxidation and electroluminescence. *J Mater Chem C*. 2014;2(34):7001–12.
18. Ma SD, Chen YL, Feng J, et al. One-step synthesis of water-dispersible and biocompatible silicon nanoparticles for selective heparin sensing and cell imaging. *Anal Chem*. 2016;88(21):10474.
19. Xia B, Zhang W, Shi J, et al. Fluorescence quenching in luminescent porous silicon nanoparticles for the detection of intracellular  $\text{Cu}^{2+}$ . *Analyst*. 2013;138(13):3629.
20. Wang Y, Wang L, Su Z, et al. Multipath colourimetric assay for copper(II) ions utilizing MarR functionalized gold nanoparticles. *Sci Rep*. 2017;7:41557.
21. Vaz R, Bettini J, Júnior JGF, et al. High luminescent carbon dots as an eco-friendly fluorescence sensor for Cr (VI) determination in water and soil samples. *J Photochem Photobiol A*. 2017;346:502–11.
22. Wang Y, Zhang P, Lu Q, et al. Water-soluble  $\text{MoS}_2$  quantum dots are a viable fluorescent probe for hypochlorite. *Microchim Acta*. 2018;185(4):233.
23. Namdari P, Negahdari B, Eatemadi A. Synthesis, properties and biomedical applications of carbon-based quantum dots: an updated review. *Biomed Pharmacother*. 2017;87:209–22.
24. Bian S, Shen C, Qian Y, et al. Facile synthesis of sulfur-doped graphene quantum dots as fluorescent sensing probes for  $\text{Ag}^+$  ions detection. *Sensors Actuators B Chem*. 2017;242:231–7.
25. Dong Y, Wang R, Li G, et al. Polyamine-functionalized carbon quantum dots as fluorescent probes for selective and sensitive detection of copper ions. *Anal Chem*. 2012;84(14):6220–4.
26. Kiy MM, Zaki A, Menhaj AB, et al. Dissecting the effect of anions on  $\text{Hg}^{2+}$  detection using a FRET based DNA probe. *Analyst*. 2012;137(15):3535–40.
27. Xie HZ, Bei F, Hou JY, Ai SY. A highly sensitive dual-signaling assay via inner filter effect between g- $\text{C}_3\text{N}_4$  and gold nanoparticles for organophosphorus pesticides. *Sensors Actuators B Chem*. 2018;255:2232–9.
28. Özyeybek G, Erarpat S, Chormey DS, et al. Sensitive determination of copper in water samples using dispersive liquid-liquid microextraction-slotted quartz tube-flame atomic absorption spectrometry. *Microchem J*. 2017;132:406–10.
29. Mergu N, Gupta VK. A novel colorimetric detection probe for copper(II) ions based on a Schiff base. *Sensors Actuators B Chem*. 2015;210:408–17.
30. Laferriere BD, Maiti TC, Arquist II, et al. A novel assay method for the trace determination of Th and U in copper and lead using inductively coupled plasma mass spectrometry. *Nucl Instrum Methods Phys Res Sect A*. 2015;775:93–8.
31. Sung TW, Lo YL. Highly sensitive and selective sensor based on silica-coated CdSe/ZnS nanoparticles for  $\text{Cu}^{2+}$  ion detection. *Sensors Actuators B Chem*. 2012;165(1):119–25.
32. Chen J, Li Y, Lv K, et al. Cyclam-functionalized carbon dots sensor for sensitive and selective detection of copper(II) ion and sulfide anion in aqueous media and its imaging in live cells. *Sensors Actuators B Chem*. 2016;224:298–306.
33. Liu X, Yang Y, Xing XX, et al. Grey level replaces fluorescent intensity: fluorescent paper sensor based on ZnO nanoparticles for quantitative detection of  $\text{Cu}^{2+}$  without photoluminescence spectrometer. *Sensors Actuators B Chem*. 2018;255:2356–66.

**Publisher's note** Springer Nature remains neutral with regard to jurisdictional claims in published maps and institutional affiliations.